CrystEngComm

Accepted Manuscript

This article can be cited before page numbers have been issued, to do this please use: M. Bazargan, M. Mirzaei, A. S. Hamid, Z. H. Kafshdar, H. Ziaekhodadadian, J. T. Mague, E. Momenzadeh, D. M. Gil, R. M. Gomila and A. Frontera, *CrystEngComm*, 2022, DOI: 10.1039/D2CE00656A.

ROYAL SOCIETY OF CHEMISTRY

rsc.li/crystengcomm

View Article Online
DOI: 10.1039/D2CE00656A

ARTICLE

On the importance of π-stacking interactions in the complexes of copper and zinc bearing pyridine-2,6-dicarboxylic acid *N*-oxide and *N*-donor auxiliary ligands

Received 00th January 20xx,
Accepted 00th January 20xx

DOI: 10.1039/x0xx00000x

Maryam Bazargan[a], Masoud Mirzaei[a,*], Abdul Samad Hamid[a,†], Zahra Heydaralizadeh Kafshdar[a,†], Hoda Ziaekhodadadian[a,†], Elham Momenzadeh[a,†], Joel T. Mague,[b] Diego M. Gil,[c] Rosa M. Gomila[d], Antonio Frontera[d,*]

Three coordination complexes $\{[Cu(pydco)(pz)_{0.5}(H_2O)]\cdot H_2O\}_n$ (**1**), $[Cu(pydco)(phen)(H_2O)]\cdot 2H_2O$ (**2**), and $[Zn_2(pydco)(phen)_2Cl_2]\cdot 2H_2O$ (**3**) have been synthesized at room temperature using a mixed-ligand system including pyridine-2,6-dicarboxylic acid *N*-oxide (H_2pydco) as *O*-donor as well as pyrazine (pz) and 1,10-phenanthroline (phen) as *N*,*N*'-bidentate donors. Single-crystal X-ray diffraction (XRD) revealed that **1** forms a 1D-coordination polymer through bridging pz units while **2** and **3** form discrete complexes in which endo-bidentate phen can only connect with one metal centre *via* a five-membered chelate ring. Also, pydco^{2-} can form a six-membered chelate ring around the metal ion *via* the *N*-oxide oxygen and one carboxylate oxygen. However, another carboxylate group of this ligand can also participate in the coordination and create unique structures in **1** and **3**. Subsequently, **1**-**3** can expand their structures into 2D-supramolecular networks through π···π stacking or H-bonding interactions. Recurrent π···π stacking motifs in all compounds have been further analyzed energetically using DFT calculations and characterized using the quantum theory of "atoms-in-molecules" (QTAIM) and noncovalent interaction plot (NCIPlot) index computational tools. In compound **3**, cooperativity effects in π···π/π···π/π···π assemblies have been also analyzed.

Introduction

Coordination compounds, as an important class of metal-containing materials, have been investigated for many years and can be classified into discrete and polymeric forms. Generally, the design and synthesis of engineered complexes require knowledge of the geometry, functional groups, and binding sites of organic ligands as well as the size and coordination behavior of metallic centres. Organic ligands can be divided into groups based on their rigid or flexible skeleton, neutral or ionic nature, chelate/bridge property, soft or hard donor atoms, and position(s) of functional groups.[1–3] Another important that tool can have a great influence on the final structure is the possibility of the formation of non-covalent interactions such as H-bonding and π-stacking interactions and their interplay that can promote the structural dimensions of the compounds.[4–6]

Despite employing a vast variety of ligands in the synthesis of new compounds, *O*/*N*-donor ligands are among the most frequent examples. Mostly, *N*-donors contain exo- and endo-*N*,*N*'-bidentate donors. In the former, ligands such as pyrazine and 4,4'-bipyridine can generate coordination polymers by forming a bridge between metal centres.[7] However, latter ligands including 1,10-phenanthrolin and 2,2'-bipyridine can form only chelate rings with metal ions thus preventing the formation of high dimensional frameworks so they are also known as terminators.[8] Among *O*-donor ligands, pyridine-based carboxylate ligands are responsible for creating thousands of compounds known not only for their structural diversity but also for their wide variety of applications in many fields from catalysts,[9,10] luminescence,[11,12] gas adsorption[13,14] to their antiproliferative activities.[15,16] For several years, pyridine-2,6-dicarboxylic acid (H_2pydco) has received considerable attention due to the symmetric position of its carboxylate groups on each side of the pyridine ring which can form 5-membered chelate rings or bridge with neighboring metal centres. Up to now, numerous metal-organic complexes, cocrystals, and salts based on this ligand have been reported. However, its *N*-oxide analogue, pyridine-2,6-dicarboxylic acid *N*-oxide (H_2pydco), is still in its early stages as a ligand (with less than 40 structures

[a] Department of Chemistry, Faculty of Science, Ferdowsi University of Mashhad, Mashhad 9177948974, Iran. E-mail: mirzaeesh@um.ac.ir.
[b] Department of Chemistry, Tulane University, New Orleans, LA, 70118, USA.
[c] . INBIOFAL (CONICET – UNT). Instituto de Química Orgánica. Facultad de Bioquímica, Química y Farmacia. Universidad Nacional de Tucumán. Ayacucho 471. T4000INI. San Miguel de Tucumán. Argentina.
[d] Departament de Química, Universitat de les Illes Balears, Crta de Valldemossa km 7.5, 07122 Palma de Mallorca (Baleares), SPAIN. E-mail: toni.frontera@uib.es
† These authors contributed equally to this work.
Electronic Supplementary Information (ESI) available: Bond distances and angles (Tables S1 and S2) and powder X-ray diffraction data (Fig. S1). See DOI: 10.1039/x0xx00000x

reported[17]) and the main focus is mainly on the synthesis and crystal habit of new structures, while systematic studies on the effects of the auxiliary ligands have not been yet explored.

In continuation of our previous work with based-oxide-*N* carboxylate compounds,[18–23] we have chosen pyrazine (pz) and 1,10-phenanthroline (phen) as based-donor-*N* ligands to survey the effect of the bridging and chelating behavior in terms of structural expansion. H_2pydco is also found to show diverse coordination modes (chelate and bridge) so it was further anticipated that it might show interesting structural properties due to its *O*-donor nature.[20,23]

In the recent past, transition metal complexes have been synthesized using H_2pydco as primary ligand and bpy or other bridging *N*-donor as auxiliary ligands [15,16]. However, according to the CSD survey, examples containing phen and pz as auxiliary ligands have not yet been reported. Here, we report the synthesis and crystal description of three coordination complexes containing H_2pydco ligand which are formulated as $\{[Cu(pydco)(pz)_{0.5}(H_2O)]\cdot H_2O\}_n$ (**1**), $[Cu(pydco)(phen)(H_2O)]\cdot 2H_2O$ (**2**) and $[Zn_2(pydco)(phen)_2Cl_2]\cdot 2H_2O$ (**3**). Also, DFT calculations combined with QTAIM and NCIplot analyses have been used to investigate the recurrent π···π stacking motifs observed in the solid state of all compounds and to study cooperativity effects in compound **3**.

Experimental

Materials and instruments

All chemicals and solvents were purchased from commercial sources and used without further purification, except for pyridine-2,6-dicarboxylic acid *N*-oxide (H_2pydco) which was synthesized according to a reported method [24]. Melting points were determined using a Barnstead Electrothermal 9300 apparatus. The infrared spectra were recorded in the range of 4000–400 cm^{-1} on a Thermo Nicolet/AVATAR 370 Fourier transform spectrophotometer using KBr pellets. Elemental analysis (CHN) was performed using a Thermo Finnigan Flash-1112 EA microanalyzer. Metal content was measured by the Spectro Arcos ICP-OES spectrometer model 76004555 using in the range of 130-770 nm for ICP spectra. Thermogravimetric analysis (TGA) was carried out under an air atmosphere from ambient temperature up to 1000 °C with a heating rate of 10 °C min^{-1} on SDT Q600 SPECIFICATIONS and Shimadzu TGA-50 instrument.

Synthesis and characterization

Synthesis of 1. A mixture of H_2pydco (0.02 g, 0.1 mmol) and pz (0.01 g, 0.1 mmol) in distilled water (6 mL) was stirred at room temperature for an hour. Then a solution of $CuCl_2.6H_2O$ (0.02 g, 0.1 mmol) in 3 mL of distilled water was added to the reaction mixture, and stirring was continued for a further 4 hours. The resulting mixture was filtered and kept at room temperature for slow evaporation. After a day, blue diamond-like crystals were obtained in 95% yield (85 mg) based on H_2pydco (m.p. 161 °C). Anal. Calcd. For $C_9H_{12}CuN_2O_7$ (%): C, 33.70; H, 2.81; N, 8.73. Found: C, 33.98; H, 2.59; N, 7.63%. FTIR (KBr pellet, cm^{-1}): 3468.36, 3389.02, 3124.04, 3088.56, 3063.77, 1643.74, 1620.32, 1596.00, 1474.47, 1421.42, 1410.90, 1395.51, 1364.14, 1244.34, 1191.89, 1158.84, 1120.84, 1067.17, 922.13, 858.65, 832.93, 780.22, 717.49, 619.62, 548.47, 472.21, 452.80.

Synthesis of 2. Compound **2** was prepared similarly to **1**, except that phen (0.04 g, 0.2 mmol) was used instead of pz. Blue needle-like crystals of **2** were obtained after 7 days by slow evaporation of the reaction mixture in a48 % yield (45 mg) based on H_2pydco (m.p. 203 °C). Anal. Calcd. For $C_{19}H_{17}CuN_3O_8$ (%): C, 47.65; H, 3.58; N, 8.77. Found: C, 46.70; H, 3.44; N, 8.62. FTIR (KBr pellet, cm^{-1}): 3401.56, 3084.20, 1698.79, 1631.98, 1584.36, 1523.06, 1428.77, 1344.26, 1276.16, 1179.92, 1079.46, 1032.64, 852.01, 771.59, 722.94, 686.94, 444.15.

Synthesis of 3. Compound **3** was prepared similarly to **2**, except that $ZnCl_2.6H_2O$ (0.03 g, 0.10 mmol) was used instead of $CuCl_2.6H_2O$. Colorless hexagonal crystals of **3** were obtained in 62 % yield (60 mg) based on phen after 10 days by slow evaporation of the reaction mixture (m.p. 247 °C). Anal. Calcd. for $C_{31}H_{23}Cl_2N_5O_7Zn_2$: C 48.78; H 2.98; N 8.99. Found: C 48.38; H 2.99; N 8.21%. IR bands (KBr pellet, cm^{-1}): 3740.3, 3424.8, 3351.2, 3162.7, 3073.9, 3053.7, 1738.2, 1637.8, 1516.5, 1425, 1353.7, 1246.2, 1221.6, 1198.3, 1143.1, 1103.6, 909.9, 847.3, 786.9, 722.7.

X-ray structure determination

Crystals of **1**-**3** were mounted on polymer loops with a drop of heavy oil and placed in the cold nitrogen stream on the diffractometer (Bruker Smart APEX for **1** and **3** and Bruker D8 Quest for **2**). Intensity data were collected under thecontrol of the *APEX3* software package [30] and the raw data were converted to F^2 values with *SAINT*[25] which also performed global refinements of the unit cell parameters. Corrections for absorption and merging of equivalent reflections were performed with *SADABS*[25] (for **1** and **3**) or *TWINABS*[26] (for **2**). The structures were solved by dual space methods (*SHELXT*[27]) and refined by full-matrix, least-squares procedures (*SHELXL*[28]). For **2**, the best crystal that could be obtained consisted of several components in random orientations with respect to one another. Based on the number of reflections attributed to each of these components, three components accounted for the majority of the measured diffraction maxima and were used in the structure determination. In the final stages, trial refinements were run using the one-component (major) reflection file extracted from the full data set with *TWINABS* and using the full, three-component reflection file. The results showed the former refinement to be more satisfactory although because of the poor crystal quality, the final structure, while clearly correct, is of low accuracy. Most hydrogen atoms were located in difference maps and were included as riding contributions in idealized positions.

Theoretical methods

The interaction energies of the assemblies studied herein were evaluated at the RI-BP86-D3/def2-TZVP[29–31] level of theory by means of the Turbomole 7.0 program[32] and using the crystallographic coordinates. The D3 dispersion[c] correction scheme was used to correct the DFT interaction energies because it is convenient for the evaluation of noncovalent interactions where π-stacking interactions are studied. The QTAIM[33] and NCIplot[34] analyses were used to

View Article Online
DOI: 10.1039/D2CE00656A

characterize the NCIs using the RI-PB86-D3/def2-TZVP wavefunction. Both the QTAIM and NCIplot analyses have been performed using the Multiwfn program[35] and represented using the VMD visualization software.[36]

Table 1. Crystallographic data and structure refinements for **1-3**.

	(**1**)	(**2**)	(**3**)
Emp. formula	$C_9H_7CuN_2O_6$·H_2O	$C_{19}H_{13}CuN_3O_6$·2(H_2O)	$C_{31}H_{19}Cl_2N_5O_5Zn_2$·2($H_2O$)
Formula weight (g/mol)	320.72	478.89	779.18
Crystal system, space group	Triclinic, *Pī*	Orthorhombic, *Pca*2_1	Orthorhombic, *Fddd*
Temperature (K)	150	125	100
a (Å)	8.1997 (8)	10.9875 (2)	18.8851 (18)
b (Å)	8.2594 (8)	12.2930 (2)	20.5134 (19)
c (Å)	9.3849 (9)	27.5133 (5)	31.983 (4)
α (°)	83.570 (1)		
β (°)	74.962 (1)		
γ (°)	64.832 (1)		
Density (Å^3)	555.55 (9)	3716.20 (11)	12390 (2)
Z	2	8	16
Radiation type	Mo Kα	Mo Kα	Mo Kα
Abs. coeff. (mm^{-1})	2.00	2.18	1.78
Crystal size (mm)	0.34 × 0.26 × 0.16	0.17 × 0.13 × 0.04	0.44 × 0.39 × 0.19
T_{min}, T_{max}	0.62, 0.74	0.70, 0.92	0.51, 0.73
No. of measured, independent and observed [$I > 2\sigma(I)$] reflections	10786, 2976, 2685	6975, 6975, 6682	58623, 4394, 3948
R_{int}	0.027	0.049	0.040
$(\sin\theta/\lambda)_{max}$ (Å^{-1})	0.690	0.618	0.698
$R[F^2 > 2\sigma(F^2)]$, $wR(F^2)$, *S*	0.025, 0.075, 1.16	0.026, 0.075, 1.04	0.029, 0.081, 1.07
No. of reflections	2976	6975	4394
No. of parameters	172	560	214
H-atom treatment	H-atom parameters constrained	H-atom parameters constrained	H-atom parameters constrained
$\Delta\rho_{max}$, $\Delta\rho_{min}$ (e Å^{-3})	0.50, −0.35	0.63, −0.38	0.59, −0.29
CCDC	1934941	2125119	1861399

Hirshfeld surfaces calculations

Hirshfeld surface analysis and their associated two-dimensional fingerprint plots are very useful methods for studying intermolecular interactions that are responsible for the crystal packing of organic and inorganic compounds.[37–39] The visualization of the intermolecular contacts in the crystal structure of complexes **1**-**3** was carried out by using the CrystalExplorer 21 software.[40] The normalized contact distance (d_{norm}) was calculated by using two distances d_e (the distance from the point to the nearest nucleus external to the surface), d_i (the distance to the nearest nucleus internal to the surface) and the van der Waals (vdW) radii of the atoms involved in the intermolecular contact. The d_{norm} values obtained from Hirshfeld surface analysis allow us to identify the different regions participating in the intermolecular interactions. Graphical plots of the Hirshfeld surfaces mapped with the d_{norm} function show a color code of red (shorter contacts), white (contacts around the sum of vdW radii of atoms), and blue (longer contacts). The Hirshfeld surfaces were mapped over a d_{norm} range of -0.35 a.u. (red) to +0.55 a.u. (blue) and shape index of -1.0 a.u. (concave) to +1.0 a.u. (convex). The 2D fingerprint plots were displated using the standard 0.6-2.4 Å range for **1** and **2**, and the translated 0.6-2.8 Å range for **3**, including reciprocal contacts.

Results and Discussion

Synthesis

Following our interest in based-oxide-*N* carboxylate compounds, we have continued our work with the synthesis of three new transition metal complexes of H_2pydco and an *N*-containing auxiliary ligand. Blue diamond-like crystals of **1** were obtained by reaction of H_2pydco and Cu^{2+} in the presence of 1,4-pyrazine under mild conditions (Scheme 1). To investigate the influence of the auxiliary ligand on the structural diversity, 1,10-phenanthroline was used in **2**. Finally, to explore the influence of a different metal on the final structure, afurther reaction was carried out using zinc cation under the same conditions. In the resulting compound **3**, a discrete complex was observed (likewise **2**) and despite several attempts to obtain suitable crystals with zinc, H_2p,ydco, and 1,4-pyrazine, only amorphous precipitates were formed. Also, powder X-ray diffraction further demonstrated the bulk purity of compounds **1**-**3** (Fig. S1).

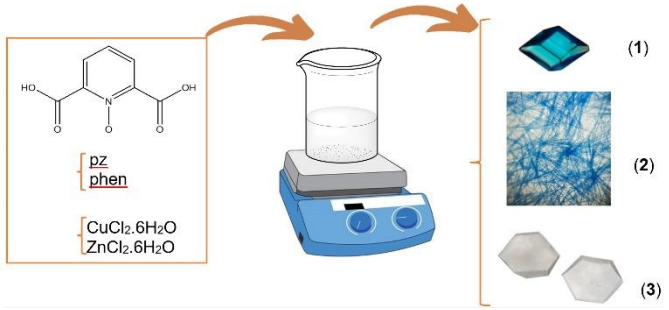

Scheme 1. (Left) Synthetic route of **1**-**3**. (Right) photographs of the crystal morphology of **1**-**3**.

IR spectra

The infrared spectra of **1-3** showed broad and strong bands at 3000–3500 cm^{-1} which can be attributed to water molecules. Also, all compounds have strong bands in the ranges 1631-1643 cm^{-1} and 1344-1364 cm^{-1}, indicating that these structures contained coordinated carboxylate groups and these bands which attributed to their asymmetric and symmetric stretching modes, respectively (Fig. S3-S5). In comparison with free H_2pydco (1754 and 1421 cm^{-1}) (Fig. S2), the strong asymmetric and symmetric stretching vibrations of the COO^- group in **1**-**3** are shifted to the lower wavenumbers, which confirms the coordination mode of this group. However, the strong band at 1698 cm^{-1} in **2** can be assigned to the uncoordinated carboxyl group of the H_2pydco. Finally, the absorption bands in the 1179–1198 cm^{-1} region are attributed to the N–O stretching vibrations of the pyridine-*N*-oxide. [41]

View Article Online DOI: 10.1039/D2CE00656A

Thermogravimetric analysis

The thermal stability of **1**-**3** was studied by thermogravimetric analysis (TGA) under an air atmosphere. TG curve of **1** showed two weight-loss (Fig. S6) in which at temperatures between 25 and 115 °C two uncoordinated and coordinated water molecules are removed amounting to 11.30 (calcd 11.25 %) and the second step occurrs from 210 to 460 °C, due to the combustion of the $pydco^{2-}$ and pz ligands with a weight loss of 68.15 (calcd. 68.43 %). For **2**, the TG curve exhibits three weight loss steps (Fig. S7), at the first step (between 25 to 108 °C) three uncoordinated and coordinated water molecules are removed with a weight loss of 11.16 (calcd. 11.29 %). Then, at the second and third steps (between 125 and 450 °C), the decomposition of the one $pydco^{2-}$ and one phen ligands with a weight loss of 74.76 (calcd. 75.10 %) occurred. For **3**, three weight-loss stages can be seen (Fig. S8). The first stage occurs between 25 and 135 °C which corresponds to the removal of two uncoordinated water molecules amounting to 4.55 (calcd 4.63 %), the second and third stages, occurring between 160 to 440 °C, are attributed to the decomposition of the one $pydco^{2-}$, two Cl^- and two phen with a weight loss of 22.50 (calcd. 23.21 %), 9.45% (calcd. 9.01 %) and 46.16% (calcd 46.33%).

Structure description of 1-3.

Single-crystal XRD and structure refinement details are summarized in Table 1. Crystallographic details can be found in the CIF files which are available free of charge from the Cambridge Crystallographic Data Centre CCDC[17] (1934941, 2125119, and 1861399). Structural analysis indicates *O*-donor $pydco^{2-}$ with bridging *N*-donor (pz) creates a coordination polymer in **1**, while with the terminator *N*-donor (phen) forms discrete complexes in **2** and **3** (Fig. 1). Selected bond distances and angles and a list of H-bond geometries are reported in Tables S1 and S2 (in the Electronic Supplementary Information file).

Structural description of 1

Complex **1** has a polymeric structure $\{[Cu(pydco)(pz)_{0.5}(H_2O)]\cdot H_2O\}_n$ and its asymmetric unit is formed of one Cu^{2+}, one $pydco^{2-}$, and half of the pz as well as one coordinated and one uncoordinated water molecule (Fig. 1a). Each copper centre shows distorted square-pyramidal coordination geometry[42] with a $CuNO_4$ formula in which the axial position is occupied by O_{water}, and the equatorial positions are occupied by N2 from pz, O1, and O5 carboxylate oxygens from two $pydco^{2-}$ ligands, and $O_{N\text{-oxide}}$ (Fig. 1). As shown in Fig. 2, two adjacent monomers are bridged by carboxylate groups to form centrosymmetric building blocks consisting of twelve-membered rings (Cu1···Cu1: 5.82 Å). These building blocks are connected to each other by pyrazine bridges to generate a 1D polymeric chain propagating in the (110) plane with the mean plane of the chain inclined by 24.7(1)° to (110) (Fig. 2). Finally, slipped, π-π stacking interactions (centroid···centroid = 3.7496(9) Å; interplanar spacing = 3.3366(6) Å, slippage = 1.71 Å) between aromatic rings link neighbouring 1D chains to each other to create 2D layers parallel to the ac plane (Fig. 3). The layers are connected by inversion related O7–H7B···O4iii hydrogen bonds (Table S2) to form the full supramolecular structure (Figs. S9 and S10).

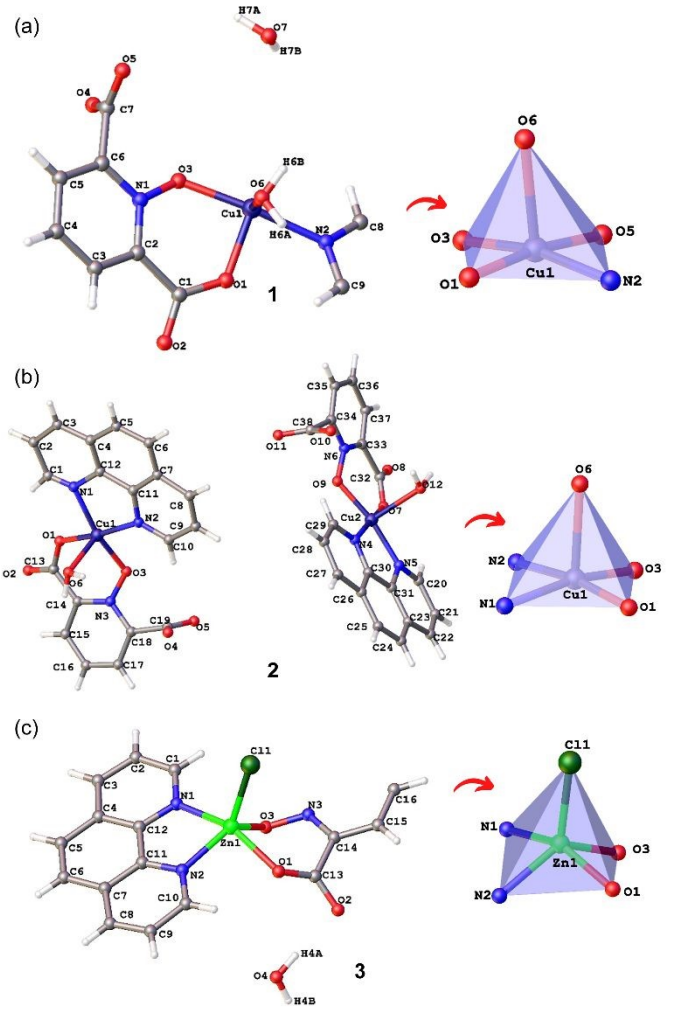

Fig. 1. (left) Asymmetric units of **1** (a), **2** (b), and **3** (c) with selected atoms labeled (uncoordinated water molecules in **2** were omitted for clarity). (right) Coordination geometry around the metal centre.

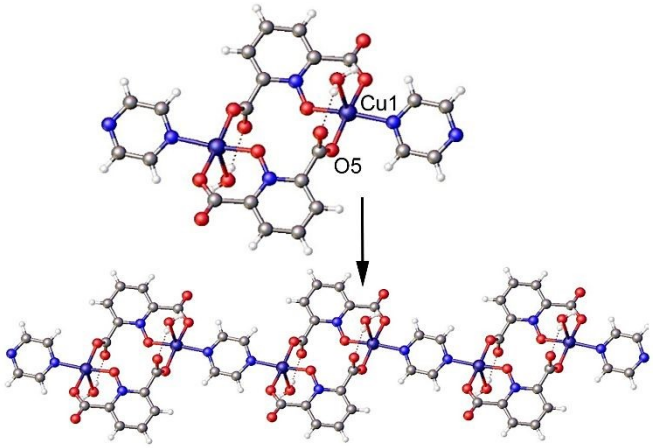

Fig. 2. (top) Building block of **1** with a twelve-membered ring (Cu1···Cu1: 5.82 Å). (bottom) 1D chain along the *a*-axis. Uncoordinated water molecules are omitted for clarity. Color code: Cu, dark blue; C, grey; N, light blue; O, red; H, white.

View Article Online
DOI: 10.1039/D2CE00656A

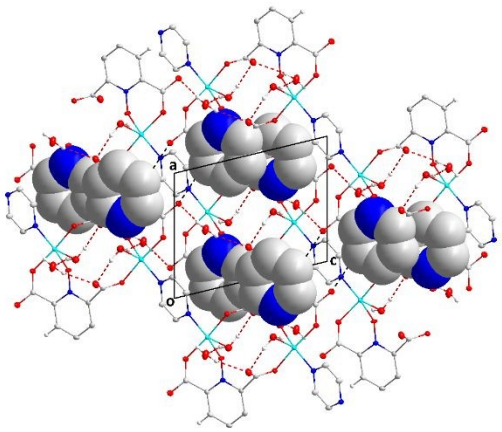

Fig. 3. 2D representation of **1** projected onto the *ac* plane formed by π-stacking interactions. Color code: Cu, light blue; C, grey; N, dark blue; O, red; H, white. Space-filling portions illustrate the π-stacking interactions.

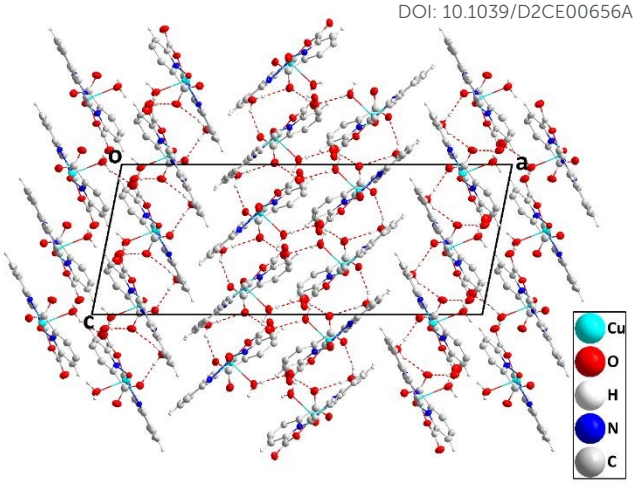

Fig. 4. A portion of three layers of molecules of **2** with O–H···O hydrogen bonds ***are*** depicted by dashed lines. Molecules containing Cu1 are in the central layer with those containing Cu2 in the outer layers.

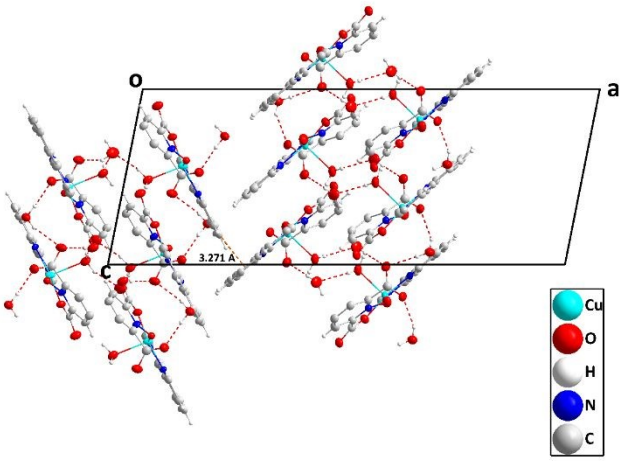

Fig. 5. A portion of two layers of molecules in **2** showing the C28–H28···Cg4 interaction as an orange dashed line with the H28···Cg4 distance labeled. The O–H···O hydrogen bonds are depicted by red dashed lines.

Structural description of 2

Complex **2** has a monomeric structure and its asymmetric unit is composed of two [Cu(pydco)(phen)(H_2O)] moieties and four uncoordinated water molecules (Fig. 1b). Both copper centres have distorted square pyramidal coordination geometry with a CuN_2O_3 formula in which the axial position is occupied by O_{water}, and the equatorial positions are occupied by two nitrogen atoms of phen, and one carboxylate and the *N*-oxide oxygen atoms of pydco^{2-} (Fig. 1b). Molecules containing Cu1 together with the lattice water molecules containing O14 and O15 are connected by O6–H6B···O15^{i}, O14–H14A···O5, O14–H14B···O4^{vi} and O15–H15B···O4 hydrogen bonds (Table S2) into layers of molecules parallel to (100). These are reinforced by π interactions between the C13=O2 group of the chelating carboxylate group and the N1/C1/C2/C3/C4/C12 ring of the phen ligand at *x*, -*y*+½, *z*-½ (O2···centroid = 3.292(13) Å, C13···centroid = 3.434(18) Å, C13=O2···centroid = 85.7(10)°. For molecules containing Cu2 and lattice water molecules containing O13 and O16, layers also parallel to (100) are generated by O12–H12A···O16, O12–H12B···O16^{iii}, O13–H13A···O11, O13–H1b···O10^{v} and O16–H16A···O10 hydrogen bonds (Table S2). Accompanying these are π interactions between C32=O8 and the N5/C20/C21/C22/C23/C31 ring of the phen ligand at *x*, -*y*+3/2, *z*-½ (O8···centroid = 3.272(15) Å, C32···centroid = 3.374(16) Å, C32=O8···centroid = 84.0(10)°) (Fig. 4). Neighboring layers are connected by the C–H···π(ring) interactions C9–H9···Cg15 and C28–H28···Cg4 where Cg4 and Cg15 are the centroids, respectively, of the N2/C10/C9/C8/C7/C11 ring at *x*, *y*, *z*+1 and the C23/C24/ C25/C26/C30/C31 ring at *x*, -*y*+3/2, *z*-½ (H9···Cg15 = 3.31 Å, C9–H9···Cg15 = 154°, H28···Cg4 = 3.27 Å, C28–H28···Cg4 = 152°) (Fig. 5). Two additional views of the supramolecular structure of 2 are presented in Figs. S11 and S12 while the individual hydrogen bond patterns are shown in Fig. S13.

Structural description of 3

Complex **3** has a dimeric structure with the [Zn_2(pydco)(phen)$_2Cl_2$]·2H_2O formula and has crystallographically-imposed C_2 rotation symmetry. The asymmetric unit of **3** contains one Zn^{2+}, half of the pydco^{2-} ligand, one phen ligand, one chloride anion, and an uncoordinated water molecule (Fig. 1c). The symmetry operation to generate the full molecule is -*x*+5/4, -*y*+5/4, *z*. The zinc centre displays a distorted square pyramidal coordination geometry with the $ZnClN_2O_2$ formula in which the axial position is occupied by a chloride ligand and the equatorial plane is occupied by two nitrogen atoms of phen and $O_{Carboxylate}$, plus $O_{N\text{-}oxide}$ of pydco^{2-} (Fig. 1). Within the dimetallic complex, there are slipped, π-stacking interactions between the phen ligands with that between the central C4/C5/C6/C7/C11/C12 rings having

View Article Online
DOI: 10.1039/D2CE00656A

centroid · · · centroid = 3.7082(11) Å, dihedral angle = 3.70(8)°, slippage = 1.26 Å. The complexes are connected by π-stacking interactions between inversion-related central C4/C5/C6/C7/C11/C12 rings to form chains of molecules extending along the [110] and [1-10] directions (centroid · · · centroid = 3.5553(10) Å, dihedral angle = 0.02(8)°, slippage = 0.82 Å) (Fig. 6). The hydrogen bonds O4–H4A···O2, O4–H4A···O2^{i} and O4^{i}–H4B^{i}···O2^{i} (symmetry code: (i): -*x*+¾, *y*, -*z*+¾) (Table S2) form chains of molecules extending along the *b*-axis direction which are linked via O4–H4B···O4^{ii} (symmetry code: (ii) *x*, -*y*+¾, -*z*+¾) hydrogen bonds (Table S2) forming layers parallel to the *ab* plane. The layers are connected along the *c*-axis direction by C3–H3···Cl1^{iii} and C3^{iv}–H3^{iv}···Cl1^{v} (symmetry codes: (iii) *x*+¼, -*y*+3/2, *z*-¼; (iv) -*x*+5/4, -*y*+5/4, *z*; (v) -*x*+1, *y*-¼, *z*-¼) hydrogen bonds (H···Cl = 2.67 Å, C–H···Cl = 147°) reinforced by C15–H15···O2^{vi} (symmetry code: (vi) -*x*+1, -*y*+1, -*z*+1) hydrogen bonds (Table S2). The 3D structure is completed by π-π stacking interactions between the central rings of the phen ligands in adjacent molecules related by -*x*+1, -*y*+3/2, -*z*+¼ (centroid···centroid = 3.5553(10) Å, slippage = 0.82 Å) and C9–H9···O2^{i} (symmetry code: (i): -*x*+¾, *y*, -*z*+¾) hydrogen bonds (Figs. 6b and Figs. S14 and S15).

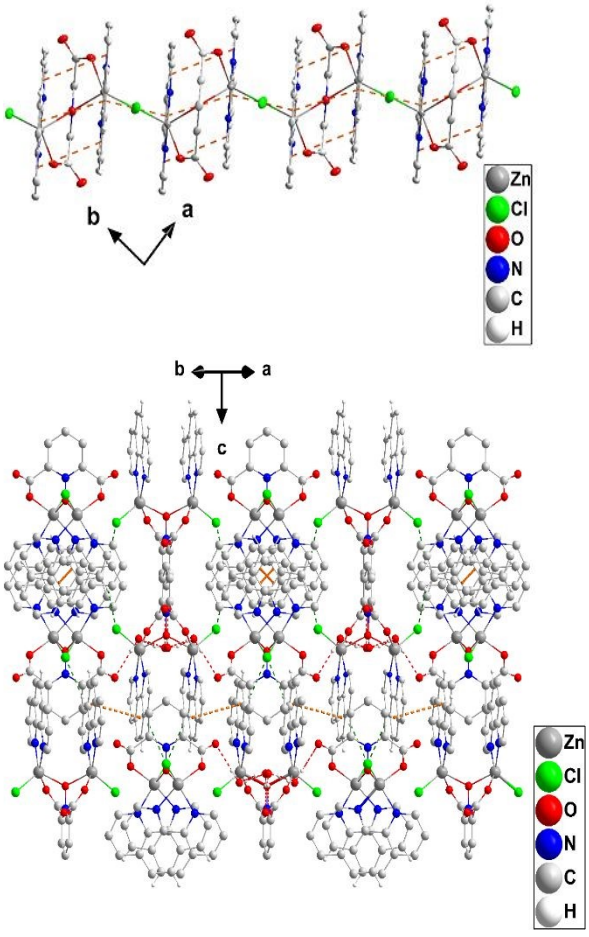

Fig. 6. top: 1D-chains of **3** created by π- π stacking interactions (orange dashed lines). Bottom: 2D-structure of **3** viewed along the [110] direction which is formed by O–H · · · O and C–H···Cl bonds (red and green dashed lines, respectively) and C–H···π interactions (orange dashed lines).

Structural comparison of 1-3

A fundamental goal of crystal engineering is to be able to understand the relationship between the molecular shape, direction of functional groups, and the possibility of intermolecular interactions in the final structure of the materials. Therefore, careful investigation of the governing factors in crystal structures is of paramount importance. For example, in ligands with more than one functional group, which one is preferred for bonding to the metal ions or for the formation of non-covalent interaction, and why? In this regard, a CSD survey can help researchers do more detailed research about structures and find logical answers to these questions. According to the CSD survey (CSD version 5.42 using ConQuest, version 2020.3.0), more than 2400 structures have been reported for pyridine-2,6-dicarboxylic acid (H_2pydc). However, for its *N*-oxide derivative, less than 40 structures have been reported so far, and none of them contain pz and phen as auxiliary ligands. It is important to note that after *N*-oxidation of the pyridine ring the molecular electrostatic potential (MEP) surfaces of pydco^{2-} and pydc^{2-} are equivalent for both ligands. Therefore, differences between these ligands arise from their different chelate ring size upon complexation and orbital effects can also explain the different behavior of both ligands.[23] In addition, steric hindrance between the carboxylate groups and the *N*-oxid moiety in pydco^{2-} leads to the rotation of one of the carboxylic acid groups from the plane of the pyridine ring and it is an important reason why this ligand mostly tends to act as a bidentate ligand [22].

Generally, the coordination behavior of pydco^{2-} can be chelating and bridging (as in **1**-**2** (Fig. 7))[21]. Although this ligand mostly prefers chelation *via* the *N*-oxide and one of the carboxylate functional groups, in some cases the other carboxylate group can also participate in the coordination mode (as in **3**). The formation of a dimeric complex in **3** can be explained by this ligand using both carboxylate groups to bind separate metal ions and the *N*-oxide group to bridge between them. Such a coordination mode would not be sterically possible for pydc^{2-}.

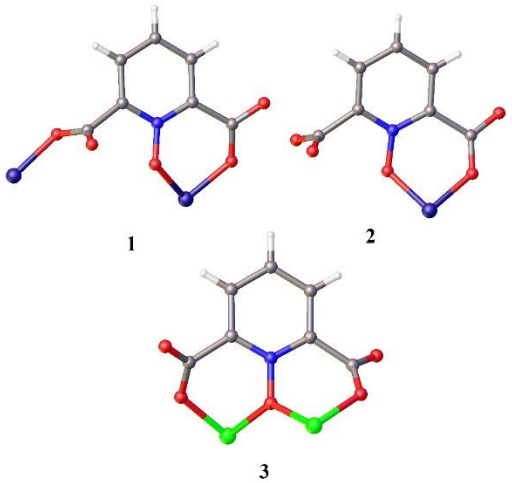

Fig. 7. Coordination modes of the pydco^{2-} ligand in the **1**-**3**. Color code: Cu, dark blue; Zn, green; C, grey; N, light blue; O, red; H, white.

Theoretical study

The theoretical study is focused on the analysis and comparison the different π-stacking modes observed in compounds **1–3** and described above in Figs. 3-6. For compound **1** we have analyzed a self-assembled dimer extracted from the ac plane shown in Fig. 3, which is represented in Fig. 8 along with the distribution of bond critical points (represented as red spheres) and the noncovalent interaction plot (NCIPlot). Only intermolecular contacts are shown for the sake of clarity. The combination of both computational tools is very convenient to reveal interactions in real space. Moreover, the NCIplot analysis also provides information regarding the attractive or repulsive nature of the interaction, which is revealed by the color of the isosurface (green-blue for attractive and yellow-red for repulsive). It can be observed that the NCIplot analysis of the dimer of **1** shows that the π-stacking is characterized by an extended green isosurface that embraces the π-cloud of the pydco^{2-} ligands. The interaction is also characterized by two bond CPs and bond paths interconnecting two C-atoms of the aromatic rings. The combined QTAIM/NCIplot analysis also discloses the existence of ancillary O···π and CH···O interactions (see Fig. 8) characterized by the corresponding bond CPs, bond paths, and green isosurfaces. The CH···O interaction is characterized by two bond CPs and bond paths connecting two aromatic H-atoms to the O-atom of the coordinated water molecule (O···H_2 bifurcated H-bond). The dimerization energy is very large (ΔE_1 = –23.3 kcal/mol) due to this intricate combination of covalent-non interactions and the antiparallel orientation of the π-stacking interaction that maximizes the dipole···dipole attraction.

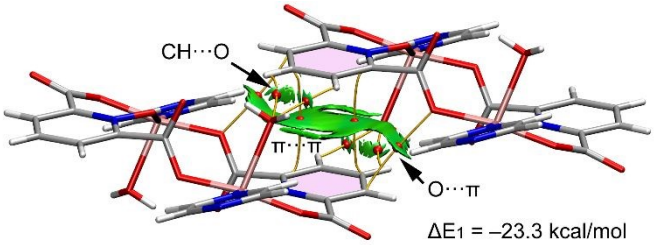

Fig. 8. Combined QTAIM (bond CPs in red and bond paths as orange lines) and NCIplot (*s* = 0.45, density cut-off = 0.04 a.u., color range –0.04 a.u. ≤ (signλ_2)ρ ≤ 0.04 a.u) for the self-assembled dimer of **1**.

For compound **2**, we have analyzed the π-stacking interaction represented in Fig. 4 that governs the formation of the 1D double chain. The QTAIM/NCIplot analysis is represented in Fig. 9, showing that the π-stacking interaction is characterized by an extended green isosurface that embraces the π-system of the phen ligand, including the five-membered chelate ring. It is worthy to comment that the dimer is also stabilized by a strong HB that connects the coordinated water molecule to one O-atom of the carboxylate group, characterized by a bond CP, bond path, and blue isosurface. The topological analysis also reveals the existence of a Cu···π interaction that is established between one Cu-atom and the central aromatic ring of the phen ligand. Finally, two O···π contacts are also revealed by the QTAIM/NCIplot analysis, as depicted in Fig. 9. The dimerization energy is very large ΔE_2 = –35.5 kcal/mol, thus confirming the importance of this assembly in the solid state of compound **2**. We have also estimated the contribution of the strong H-bond by using the value of the potential energy density (Vr) at the bond CP that characterizes this H-bond and using the equation proposed by Espinosa et al (E = 0.5 x V_r).[43] The resulting binding energy is indicated in Fig. 9 using a red-coloured font (–6.5 kcal/mol), confirming the strong nature of this contact. The contribution of the π-interactions (π···π, O···π, and Cu···π) can be thus estimated in –29.0 kcal/mol, which is stronger than the dimerization energy of the π-stacked dimer of compound **1**, in line with the larger overlap of the π-systems in compound **2**.

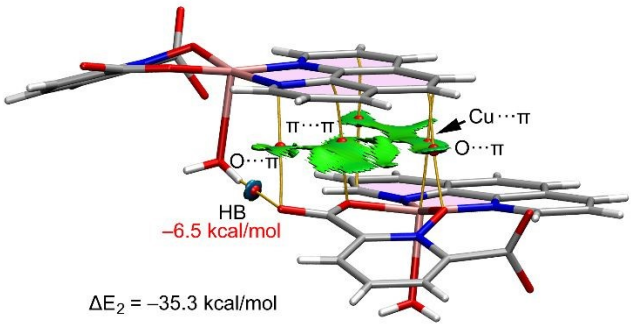

Fig. 9 Combined QTAIM (bond CPs in red and bond paths as orange lines) and NCIplot (*s* = 0.45, density cut-off = 0.04 a.u., color range –0.04 a.u. ≤ (signλ_2)ρ ≤ 0.04 a.u) for the dimer of **2**. The H-bond association energies estimated using (Vr) are indicated in red.

Finally, for compound **3**, the effect of the intramolecular π···π stacking interaction upon the intermolecular π···π interaction has been analyzed. To do so, we have studied two dimers, one corresponding to the real system (assembly shown in Fig. 10a) and the other one to a mutated dimer (Fig. 10b). In the real one, a π···π/π···π/π···π assembly is formed (two intramolecular and one intermolecular π···π interactions), as represented in Fig. 10a. The existence of both intra and intermolecular π-stacking interactions is confirmed by the NCIplot analysis that shows very large green isosurfaces that embrace the region between both phen ligands, including the chelate rings. The binding energy of this assembly is very large (ΔE_3 = –31.3 kcal/mol) due to the antiparallel orientation and large overlap of the π-systems.

To study the influence of the intramolecular π-stacking interaction upon the intermolecular one, we have constructed a mutated dimer where one of the Zn(phen)Cl fragments of each monomer has been eliminated (see Fig. 10b) to eliminate the intramolecular π···π interaction. Moreover, one of the carboxylate groups of the pydco^{2-} ligand has been protonated to keep the charge of the system neutral (see small arrows in Fig. 10b). The dimerization energy of the mutated dimer is smaller (ΔE_4 = –26.0 kcal/mol) than that of the whole system, suggesting a favorable cooperativity effect between both π-stacking interactions. The QTAIM/NCIPlot analysis also reveals the existence of ancillary CH···Cl contacts. We have evaluated its contribution using the V_r energy predictor, evidencing that they are weak (–0.7 and –0.8 kcal/mol), thus confirming that the

View Article Online
DOI: 10.1039/D2CE00656A

formation of the dimer is largely dominated by the π-stacking interactions.

The π-stacking interaction analysed in compounds **1–3**, are significantly stronger than those observed in organic compounds.[44] For instance, the stabilities of benzene-naphthalene and the naphthalene dimers are –4.2 and –6.2 kcal/mol, respectively.[45] This is due to the strong influence of the metal centers (increasing the dipole···dipole interaction). Moreover, the presence of heteroatoms[45] and the chelate rings[46] in compounds **1–3** also reinforce the π-stacking interaction, as previously demonstrated.[46]

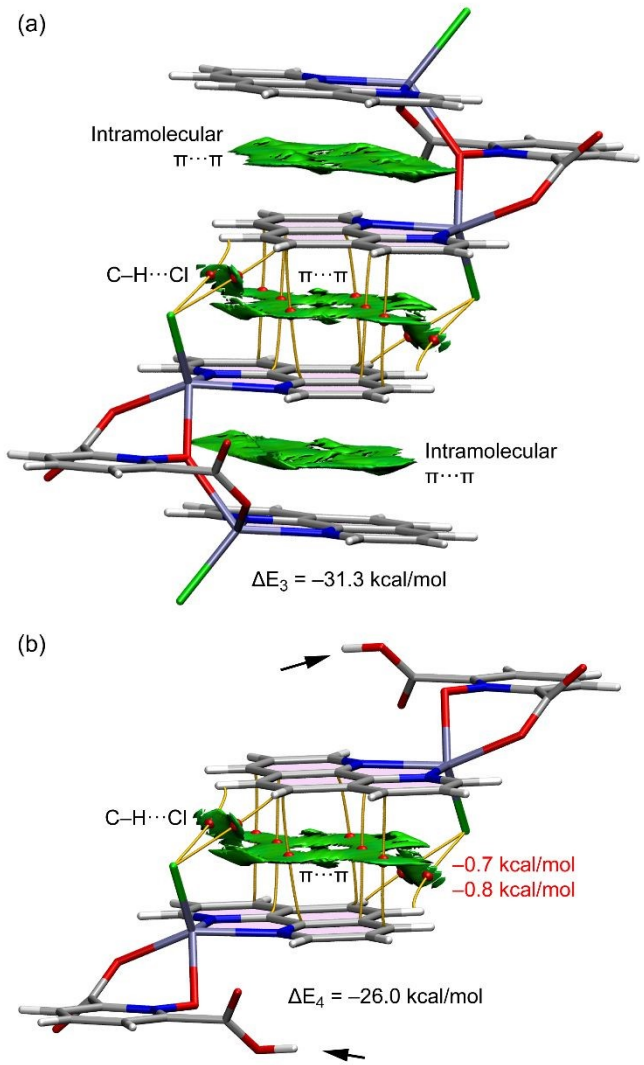

Fig. 10. Combined QTAIM (bond CPs in red and bond paths as orange lines) and NCIplot (s = 0.45, density cut-off = 0.04 a.u., color range –0.04 a.u. ≤ (signλ_2)ρ ≤ 0.04 a.u) for the self-assembled dimer of **3** (a) and the mutated dimer (b). The H-bond association energies estimated using the potential energy density (Vr) are indicated in red next to the bond CPs.

Hirshfeld surface analysis

A view of the Hirshfeld surfaces mapped over d_{norm} property is shown in Fig. 11, highlighting the main intermolecular interactions and scheme of labels. The surfaces are shown in transparent to allow visualization of the molecular moiety. We have considered the asymmetric unit among the entire unit cell for complexes **1-3**. The full fingerprint plot for 1-3 are depicted in Fig. 12.

For **1**, the two bright-red regions labeled 1 and 2 in the d_{norm} map (Fig. 11) indicate H···O/O···H contacts attributed to O6-H6A···O7 and O7-H7A···O2 hydrogen bonds, respectively. The former contact is associated to the interaction between the H-atom of the coordinated water molecule and the O2 atom of the pydco ligand, while the later involves the H7A atom of the non-coordinated water molecule and the O2 of the pydco ligand. The red spots labeled 3 in the Hirshfeld surfaces are attributed to C3-H3···O2 hydrogen bonds, involving the H3 atom of the pyridine ring and the O2 atom of the pydco ligand as acceptor. The H···O/O···H contacts, represented as spikes labeled 1 in the fingerprint plot of **1** (Fig. 12) comprise 38.9% of the total Hirshfeld surface area.

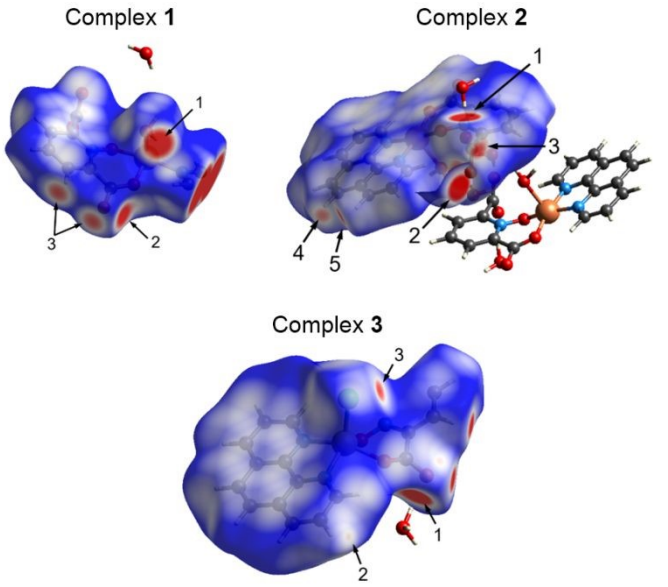

Fig. 11. A view of the Hirshfeld surfaces of **1-3** mapped over d_{norm} function. The labels are described in the main text.

In complex **2**, the two largest circular red areas labeled 1 and 2 (Fig. 11) represent H···O/O···H contacts, which are attributed to strong O13-H13B···O4 and O6-H6A···O15 hydrogen bonds, being the later the interaction between coordinated and non-coordinated water molecules. The smaller red spots regions labeled 3, 4 and 5 are indicative of weaker C10-H10···O4, C13-H13···O14 and C15-H15···O14 hydrogen bonds. The intermolecular H···O/O···H contacts (labeled 1 in Fig. 12) appear as a pair of symmetrical spikes in the fingerprint plots around (d_e + d_i) ≈ 1.8 Å, comprising 31.2% of the total Hirshfeld surface area, whereas the intermolecular H···C/C···H contacts (labeled 3) constitute the second most dominant interactions (17.3%). These contacts are mainly associated to C-H···π interactions, as was described previously. The fingerprint plot of **2** also shows O···C/C···O contacts associated to intermolecular O···π interactions, with 8.6% of contribution to the total Hirshfeld surface area.

Hirshfeld surfaces of **3** mapped over d_{norm} show a large red spot (labeled 1 in Fig. 11) associated to O4-H4A···O2 hydrogen bonds involving the H-atom of the non-coordinated water molecule and the O2 atom of the carboxylate moiety as acceptor, whereas the small

region labeled 2 is attributed to weak C9-H9···O2 hydrogen bonds. The H···O/O···H interactions comprise 17.5% of the Hirshfeld surface of this molecule. H···Cl/Cl···H contacts (labeled 4 in Fig. 12) appear as a pair of spikes at ($d_e + d_i$) ≈ 2.6 Å and comprise 16.3% of the Hirshfeld surface area. In addition, these interactions are also visible in the d_{norm} map (Fig. 11) as red spots labeled 3 associated to intermolecular C3-H3···Cl1 hydrogen bonds.

The H···H contacts also operate in the crystal packing of the three compounds. These interactions comprise 22.5, 32.0 and 26.1% of the total Hirshfeld surface area for **1**, **2** and **3**, respectively.

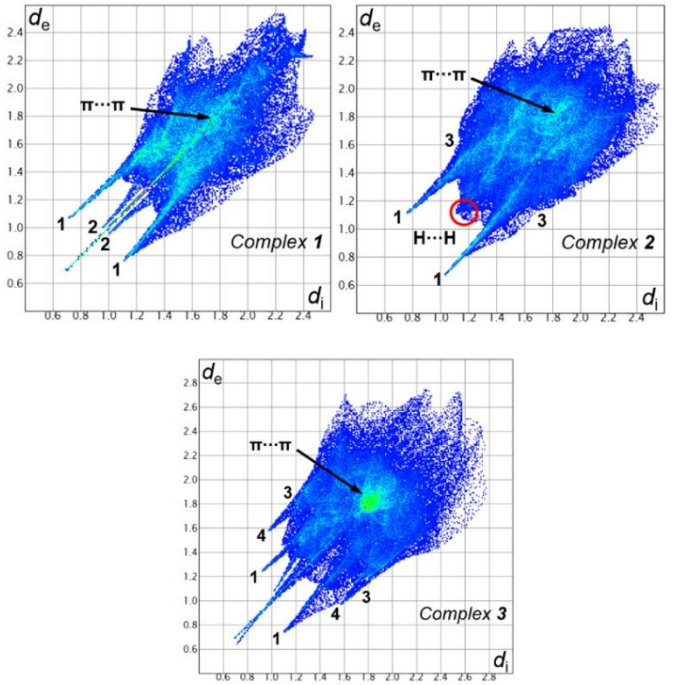

Fig. 12. Full two-dimensional fingerprint plots for **1**-**3** showing (1) H···O/O···H, (2) Cu···O, (3) H···C/C···H, and (4) H···Cl/Cl···H contacts.

To examine the influence of π···π stacking interaction in the molecular packing of complexes, we have examined the Hirshfeld surfaces mapped over *shape index* and *curvedness* (Fig. S16). The pattern of touching red and blue triangles on the *shape index* surfaces (highlighted in dashed circles) and the flat region delineated by the blue outline above the corresponding π-system on curvedness are mainly attributed to π···π stacking interactions.[47]

Conclusion

In summary, by a systematic combination of *N*- and *O*-donor ligands in a mixed-ligand system, three coordination complexes have been successfully synthesized and structurally characterized by single-crystal XRD. Due to the different nature of *N*, *N*'-bidentate auxiliary ligands a 1D-coordination polymer and two discrete compounds are formed by pz and phen. Moreover, the *N*-oxide moiety of pydco^{2-} not only provides the novelty of this work, but also enriches the structural diversity in **1**-**3** by its unique coordination modes.

The energetic features of the π-stacking interactions have been studied, showing that they are strong binding motifs in all complexes. In **3**, favorable cooperativity effects between intra and intermolecular π···π interactions have been demonstrated, thus suggesting that they can be used in crystal engineering to construct highly ordered solid state structures. We expect that the results reported herein combining theory and experiment can be useful to researchers working in supramolecular chemistry, crystal engineering as well as theoreticians.

Author Contributions

M. B.: Methodology, Formal analysis, Investigation, Data curation, Writing-original draft preparation. M. M.: Conceptualization, Funding acquisition, Main idea, Supervision, Writing-review and editing, Project administration, Visualization. A. S. H.: Experimental work, Methodology. Z. H. K.: Experimental work, Methodology. H. Z.: Experimental work, Methodology. E. M.: Experimental work, Methodology. J. T. M.: Crystallographer, Writing-review and editing. R. M. G.: DFT studies. A. F.: DFT studies, Funding acquisition, Supervision, Writing-review-review and editing, Project administration, Visualization. D. M. G.: Hirshfeld surface analysis study.

Conflicts of interest

There are no conflicts to declare.

Acknowledgments

M.M. gratefully acknowledges financial support from the Ferdowsi University of Mashhad (Grant No. 3/50211, 46881, and 50202), the Iran Science Elites Federation (ISEF), Zeolite and Porous Materials Committee of Iranian Chemical Society, and the Iran National Science Foundation (INSF). M.M. also acknowledges the Cambridge Crystallographic Data Centre (CCDC) for access to the Cambridge Structural Database. This work is supported by Iran Science Elites Federation Grant No. M/98208, M/99397, and M/400230. J.T.M thanks Tulane University for support of the Tulane Crystallography Laboratory. A. F. thanks the MICIU/AEI from Spain for financial support (Project PID2020-115637GB-I00, FEDER funds).

Notes and references

1 R. J. Lundgren and M. Stradiotto, eds. M. Stradiotto and R. J. Lundgren, John Wiley & Sons, Ltd, Chichester, UK, 2016, pp. 1–14.
2 J. R. Lundgren and Stradiotto Mark, *Ligand Design in Metal Chemistry: Reactivity and Catalysis*, John Wiley & Sons, Ltd, Chichester, UK, 2016.
3 N. Ogiwara, H. Kobayashi, M. Inukai, Y. Nishiyama, P. Concepción, F. Rey and H. Kitagawa, *Nano Lett.*, 2020, **20**, 426–432.
4 I. Alkorta, J. Elguero and A. Frontera, *Crystals*, 2020, **10**, 180.
5 S. Roca, L. Hok, R. Vianello, M. Borovina, M. Đaković, L. Karanović, D. Vikić-Topić and Z. Popović, *CrystEngComm*, 2020, **22**, 7962–7974.

6 K. T. Mahmudov, A. V. Gurbanov, F. I. Guseinov and M. F. C. Guedes da Silva, *Coord. Chem. Rev.*, 2019, **387**, 32–46.
7 M. Bazargan, M. Mirzaei and M. Akbari, *J. Mol. Struct.*, 2019, **1188**, 129–141.
8 M. Bazargan, M. Mirzaei, A. Franconetti and A. Frontera, *Dalton Trans.*, 2019, **48**, 5476–5490.
9 G. M. Rodriguez, F. Zaccaria, S. Van Dijk, C. Zuccaccia and A. Macchioni, *Organometallics*, 2021, **40**, 3445–3453.
10 R. Pandey, D. Singh, N. Thakur and K. K. Raj, *ACS Omega*, 2021, **6**, 13240–13259.
11 X.-Y. Zhao, H. Yang, W.-Y. Zhao, J. Wang and Q.-S. Yang, *Dalton Trans.*, 2021, **50**, 1300–1306.
12 C.-X. Zhao, X.-P. Zhang, Y. Shu and J.-H. Wang, *ACS Appl. Mater. Interfaces*, 2020, **12**, 22593–22600.
13 M. Sato, T. Ishigaki, M. Iwaki, K. Uematsu, M. Watanabe and K. Toda, *Inorg. Chem.*, 2021, **60**, 17810–17823.
14 L. Fan, S. Lin, X. Wang, L. Yue, T. Xu, Z. Jiang and Y. He, *Inorg. Chem.*, 2021, **60**, 2704–2715.
15 H. S. Moradi, E. Momenzadeh, M. Asar, S. Iranpour, A. R. Bahrami, M. Bazargan, H. Hassanzadeh, M. M. Matin and M. Mirzaei, *J. Mol. Struct.*, 2022, **1249**, 131584.
16 H. Alizadeh, M. Mirzaei, A. S. Saljooghi, V. Jodaian, M. Bazargan, J. T. Mague, R. M. Gomila and A. Frontera, *RSC Adv.*, 2021, **11**, 37403–37412.
17 C. R. Groom, I. J. Bruno, M. P. Lightfoot and S. C. Ward, *Acta Cryst.Sect.* , 2016, **72**, 171–179.
18 M. Mirzaei, F. Sadeghi, K. Molčanov, J. K. Zaręba, R. M. Gomila and A. Frontera, *Cryst. Growth Des.*, 2020, **20**, 1738–1751.
19 Z. Hosseini-Hashemi, M. Mirzaei, A. Jafari, P. Hosseinpour, M. Yousefi, A. Frontera, M. Lari Dashtbayaz, M. Shamsipur and M. Ardalani, *RSC Adv.*, 2019, **9**, 25382–25404.
20 M. Mirzaei, H. Eshtiagh-hosseini, M. Bazargan, F. Mehrzad, M. Shahbazi, J. T. Mague, A. Bauzá and A. Frontera, *Inorg. Chim. Acta*, 2015, **438**, 135–145.
21 M. Mirzaei, H. Eshtiagh-Hosseini and M. Bazargan, *Res. Chem. Intermed.*, 2015, **41**, 9785–9803.
22 M. Bazargan, M. Mirzaei, H. Eshtiagh-Hosseini, J. T. Mague, A. Bauzá and A. Frontera, *Inorg. Chim. Acta*, 2016, **449**, 44–51.
23 M. Bazargan, M. Mirzaei, M. Aghamohamadi, M. Tahmasebi and A. Frontera, *J. Mol. Struct.*, 2020, **1202**, 127243.
24 L. Syper, K. Kloc and J. Mz.xl;lochowski, *Tetrahedron*, 1980, **36**, 123–129.
25 APEX3, SADABS and SAINT, Bruker-AXS, Madison, 2016.
26 G. G. M. Sheldrick, TWINABS, University of Göttingen.
27 G. M. Sheldrick, *Acta Cryst.*, 2015, **A71**, 3–8.
28 G. M. Sheldrick, *Acta Cryst.*, 2015, **C71**, 3–8.
29 C. Adamo and V. Barone, *J. Chem. Phys.*, 1999, **110**, 6158–6170.
30 F. Weigend, *Phys. Chem. Chem. Phys.*, 2006, **8**, 1057.
31 S. Grimme, J. Antony, S. Ehrlich and H. Krieg, *J. Chem. Phys.*, 2010, **132**, 154104.
32 R. Ahlrichs, M. Bär, M. Häser, H. Horn and C. Kölmel, *Chem. Phys. Lett.*, 1989, **162**, 165–169.
33 R. F. W. Bader, *Chem. Rev.*, 1991, **91**, 893–928.
34 J. Contreras-García, E. R. Johnson, S. Keinan, R. Chaudret, J.-P. Piquemal, D. N. Beratan and W. Yang, *J. Chem. Theory Comput.*, 2011, **7**, 625–632.
35 T. Lu and F. Chen, *J. Comput. Chem.*, 2012, **33**, 580–592.
36 W. Humphrey, A. Dalke and K. Schulten, *J. Mol. Graph.*, 1996, **14**, 33–38.
37 J. J. McKinnon, M. A. Spackman and A. S. Mitchell, *Acta Cryst. Sect. B*, 2004, **60**, 627–668.
38 M. A. Spackman and D. Jayatilaka, *CrystEngComm*, 2009, **11**, 19–32.
39 M. A. Spackman, *Chem. Rev.*, 1992, **92**, 1769–1797.
40 P. R. Spackman, M. J. Turner, J. J. McKinnon, S. K. Wolff, D. J. Grimwood, D. Jayatilaka and M. A. Spackman, *J. Appl. Crystallogr.*, 2021, **54**, 1006–1011.
41 K. Nakamoto, in *Handbook of Vibrational Spectroscopy*, ed. P. R. Griffiths, John Wiley & Sons, Ltd, Chichester, UK, 2006, pp. 1872–1892.
42 A. W. Addison, T. N. Rao, J. Reedijk, J. van Rijn and G. C. Verschoor, *J. Chem. Soc., Dalt. Trans.*, 1984, **17**, 1349–1356.
43 E. Espinosa, E. Molins and C. Lecomte, *Chem. Phys. Lett.*, 1998, **285**, 170–173.
44 E. G. Hohenstein and C. D. Sherrill, *J. Phys. Chem. A*, 2009, **113**, 878 - 8865.
45 M. Rubeš, O. Bludský and P. Nachtigall, *ChemPhysChem*, 2008, **9**, 1702-1708.
46 (a) D. P. Malenova, G. V. Janjić, V. B. Medaković, M. B. Hall and S. D. Zarić, *Coord. Chem. Rev.*, 2017, **345**, 318-341; (b) D. P. Malenov and S. D. Zarić, *Dalton Trans.*, 2019, **48**, 6328-6332; (c) P. V. Petrovic, G. V. Janjic and S. D. Zaric, *Cryst. Growth Des.*, 2014, **14**, 3880- 3889
47 M. A. Spackman, *Phys. Scr.*, 2013, **87**, 048103.